A New GNSS-based Approach for Volcanic Vent Location during Lava Fountains

Flavio Cannavó, Massimo Aranzulla, Simona Scollo, Giuseppe Puglisi

***Abstract*—Recent studies have focused on the capability of Global Navigation Satellite System (GNSS) instruments to detect volcanic plumes by means of either variation in signal-to-noise ratio or products from positioning processing. These new approaches in volcanic plume detection can be extremely useful for volcanoes worldwide, which may not have advanced monitoring systems or during bad weather conditions when other video and satellite techniques may fail. In this paper, we show how the GNSS stations can provide a new tool to locate the volcanic vent during highly explosive events. The proposed method has been tested on the lava fountains at Mt. Etna, in Italy, that since 2011 have characterized most of the eruptive activity and have involved different volcanic vents. Our results confirm that not only is there evidence of detectable interaction between volcanic plumes and GNSS data, but also, for the first time on a large dataset we are able to discriminate the erupting vent with great precision.**

***Index Terms*—GNSS, Lava Fountains, Eruption Columns, Vent Location.**

I. Introduction

A VOLCANIC eruption is one of the largest energy-release phenomena known on Earth. Among the different styles of eruptions, explosive activities are often the most powerful and can produce high eruption columns of hot volcanic particles mixed with volcanic gas that vary in quantity depending on the eruption styles [1]. Eruption columns, ejected into the atmosphere at speeds of several hundred meters per second [1]–[3], can rise up to several kilometers above the vent and can lead to different types of hazards. The most important is undoubtedly the hazard to aviation because volcanic ash can damage the engines causing, in the worst case, their failures [4].

Since most volcanic clouds are not detectable by radars aboard the aircraft, a network of nine Volcanic Ash Advisory Centers around the world was set up by the International Civil Aviation Organisation (ICAO) to coordinate and disseminate information on atmospheric volcanic ash clouds that may endanger aviation. Information and decisions are based on the continuous monitoring of volcanic plumes using data from satellites, volcanological observatories, pilot reports and numerical volcanic ash forecasts. Another important hazard due to eruption columns is their possible collapse, especially in highly explosive volcanoes (e.g. Mt. Vesuvius, Italy; Mt. St. Helens, USA). Indeed, eruption columns may collapse when the rate at which magma is erupted rises to a point where insufficient air ascends to support it. Material reaching the bottom of the convective lift region can then no longer be sufficiently supported by convection and will fall under the force of gravity, forming a pyroclastic flow that can travel down the flanks of a volcano at speeds of over 100 km/h [5]. Although related to the magma properties and eruption characteristics, the column collapse depends closely on the vent radius and geometry [6], [7]. In addition to geometry, the vent location is critical to determine the pyroclastic flow invasion areas, hence justifying the importance of rapidly locating the erupting vent. A further hazard linked to vent location during eruptions concerns possible heavy bomb fallout formed during powerful lava fountains that may injure people and damage tourist facilities [8].

Overall, the locating of active vents during explosive activities becomes crucial to assess the hazardous areas for all those adverse phenomena. To this end, analysis of volcanic tremor, generated by the movement of magma below and/or within the volcano edifice, is widely used to locate the volcanic source [9]. However, the method cannot currently determine the exact position of the active vent during explosive activity. A more useful parameter for active vent detection is the acoustic signal, especially in the infrasound band [10], [11], that allows locating the source with great precision by means of techniques like semblance [12], [13] or Bayesian approaches [14]. Finally, video systems based on visible and thermal cameras, which are extensively adopted in volcano observatories for surveillance purposes [15], are able to retrieve a lot of information on eruptive activity in cloudless conditions.

In this letter, we use the recently developed technique to detect volcanic plumes [16], based on variations of GPS signal features, to help identify the area affected by the eruption column and, consequently, locate the volcanic active vent.

The method was tested at Mt. Etna, in Italy, where 49 lava fountains have occurred since 2011 from different volcanic vents.

II. Sensing Paroxysmal Activity by GNSS

Today, Global Navigation Satellite System (GNSS) receivers are commonly installed around active volcanoes to measure surface displacements related to volcano dynamics such as inflation/deflation processes and eruptive intrusions. Some studies have proven another utility of GNSS stations in detecting volcanic plumes ejected from large explosive events. Indeed, Grapenthin *et al.* [17] for the 2009 eruption of Redoubt volcano (Alaska) and Aranzulla *et al.* [18] for Mt. Etna (Italy) on September 2007, have shown that standard geodetic

F. Cannavó, M. Aranzulla, G. Puglisi and S. Scollo are with Istituto Nazionale di Geofisica e Vulcanologia, Osservatorio Etneo, Piazza Roma 2, 95123 Catania, Italy, e-mail: flavio.cannavo@ingv.it

Manuscript received ....; revised ....

techniques can sense volcanic plumes in the studied cases as atmospheric effects that, altering the GPS signal, affect the postfit phase residuals of basic GPS positioning processing.

In the last few years, an innovative and promising technique related to GPS signal strength, originally proposed by Larson [16] in 2013, has been tested to detect volcanic plumes at different volcanoes, such as Mt. Redoubt volcano (for the eruption in 2009), Mt. Etna in Italy (23 November 2013 lava fountains) [19], and Sakurajima [20] in Japan (for the eruption on 24 July, 2012). The technique is based on attenuation of the measured and recorded signal-to-noise ratio (SNR), observed in some cases at the GPS receivers during periods of volcanic plume coverage [16].

III. Method for Eruption Column Location by GNSS

The proposed method for eruption column location, and consequently vent location, exploits exploits the SNR attenuation of direct GPS satellite microwave signals in the presence of dense volcanic plumes in the atmosphere [16]. For the designed GPS working frequency bands, the SNR signal of the two carrier waves (namely L1 and L2) should not be sensitive to water vapor variations, and the direct signal can only be attenuated if there are passive anomalies in a dissipative environment. Moreover, for the same physical reason, the SNR should not interfere with small inert particles like volcanic ash, but could be sensitive to the aggregation of ejected objects inside eruption columns or filtered by the formation of liquid due to water vapor condensation in the rising eruption column [21]. Indeed, because of the physical interaction with aggregated materials and liquid water, the eruption column is potentially and likely the major medium affecting the SNR at the GPS frequency bands.

With these assumptions, the proposed approach for vent location during paroxysms consists of a two-step filtering: a filter on attenuation strength of SNR and a geometric filter to focus on concentrated/polarized rays crossing the area where paroxysms occur.

Let $S_{xy}(t)$ be the SNR time series (both for L1 and L2 bands) recorded at a ground GPS station x and relative to the satellite y. To highlight potential statistical anomalies in the SNR signal, we apply a time series normalization as expressed in Eq. (1)

$$\tilde{s}_{xy}(t) \triangleq -\frac{S_{xy}(t) - \mu_{S_{xy}}(t)}{\sigma_{S_{xy}}(t)} \tag{1}$$

by defining the two new time series of features of average and standard deviation as expressed in Eqs. (2) and (3),

$$\mu_{S_{xy}}(t) \triangleq \sum_{i=1}^{n} k_i S_{xy}\left(t - \tau(t,y,i)\right) \tag{2}$$

$$\sigma_{S_{xy}}(t) \triangleq \sqrt{\frac{1}{n}\sum_{i=1}^{n}\left[S_{xy}\left(t - \tau(t,y,i)\right) - \mu_{S_{xy}}(t)\right]^2} \tag{3}$$

where n is the number of regressors (i.e. number of past values of SNR considered in the normalization), $\tau(t,y,i)$ is the i-th time shift (greater than $23 \cdot i$ hours) that minimizes the distance between the position of satellite y at time $t - \tau(t,y,i)$ and the actual position at time t. Typically, $\tau(t,y,i)$ corresponds to i times the sidereal day of 23.9344696 hours [22].

Let T^q be the set of the times when the volcano is quiescent. We choose the number of regressors n and the coefficients $k_1, ..., k_n$ that minimize the signal fluctuations in quiescence condition (i.e. its root mean squared errors, RMSE), as shown in Eq. (4).

$$[k_1, ..., k_n] = \underset{k_1,...,k_n}{\arg\min}\left\{RMSE^q_{xy}\right\} \tag{4}$$

where

$$RMSE^q_{xy} = \int_{t\in T^q}\left[S_{xy}(t) - \mu_{S_{xy}}(t)\right]^2 \tag{5}$$

1) Strength Filtering: Let T^f be the set of the times of a single eruption f when the volcano is erupting and an eruption column is forming. We select the times $T^f_{xy} \subseteq T^f$ when the variation on the SNR for the pair (x,y) exceeds the statistical threshold of κ times the estimated standard deviation from the average value:

$$T^f_{xy} \triangleq \left\{t \in T^f | \tilde{s}_{xy}(t) \geq \kappa\right\} \tag{6}$$

In order to highlight clear evidence of polarized anomalies on the SNR signal, we subsequently apply a geometrical filtering technique as follows.

2) Geometrical Filtering: We calculate the mean azimuth of the satellite-station rays for the statistically "anomalous" time (i.e. the time when SNR signal shows statistical anomalies in strength) during the eruption:

$$\bar{\alpha}^f_{xy} = arg\left(\int_{T^f_{xy}} e^{j\alpha_{xy}(t)}dt\right) \tag{7}$$

where $\alpha_{xy}(t)$ is the azimuth of satellite y with respect to the ground station x at the time t, and j is the imaginary unit. To the mean azimuth in Equation (7) we associate a standard deviation to estimate the azimuthal dispersion of "anomalous" rays calculated by

$$\sigma^f_{\alpha_{xy}} = \sqrt{\frac{1}{\left\|T^f_{xy}\right\|}\int_{T^f_{xy}} arg^2\left(e^{j\left(\alpha_{xy}(t) - \bar{\alpha}^f_{xy}\right)}\right)dt} \tag{8}$$

where $\|\cdot\|$ is the cardinality operator.

We define the geometric filter as the filter on azimuthal dispersion of rays as follows:

$$\begin{aligned}\Psi^f_{xy} = \Big\{&\tilde{s}_{xy}(t)\cdot e^{j\alpha_{xy}(t)} | t \in T^f_{xy} \wedge \\ &\left|\alpha_{xy}(t) - \bar{\alpha}^f_{xy}\right| \leq \sigma^f_{\alpha_{xy}} \leq \frac{\pi}{6}\Big\}\end{aligned} \tag{9}$$

Thus, the final set Ψ^f_{xy} contains the vectors defined by the azimuth of the satellite-station rays and the magnitude of the related anomalous normalized SNR value.

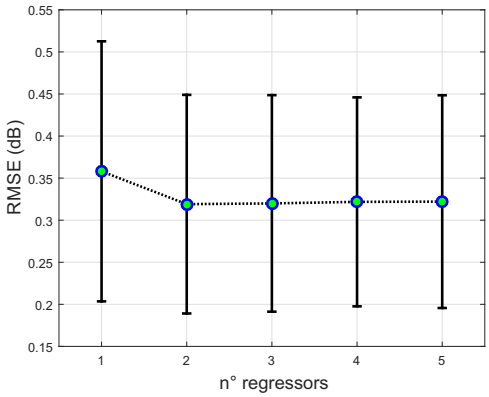

Fig. 1. Mean and standard deviation of the RMSE of the optimally normalized SNR signals (i.e. $\tilde{s}_{xy}(t)$) by Eq. (4) for different numbers of regressors, n in Eqs. (2) and (3).

Moreover, we consider the anomalies reliable when they are not single isolated spikes, but rather when they show repeatability through time for at least 2 minutes, in other words when $\left\|\Psi_{xy}^{f}\right\| \geq 4$ (for the common data sampling period of 30 seconds), and we call Ψ_{x}^{f} the set of all the Ψ_{xy}^{f} of a single station x for all the possible satellites.

IV. Results and Discussion

We have applied the described method by analysing the SNR data from the permanent stations of the Etnean GPS network, run by Istituto Nazionale di Geofisica e Vulcanologia, Osservatorio Etneo, in light of data coming from the recent lava fountains [19]. Explosive activity at Mt. Etna, in Italy, is often characterized by a paroxysmal phase in which powerful lava jets produced high eruption columns, usually going beyond the troposphere ($\sim 11/12$ km above sea level (a.s.l.)) and forming a copious tephra fallout on volcano flanks. Due to its frequent eruptions and the great availability of data, to test the proposed method, we have analyzed the 49 highly explosive events producing columns on Mt. Etna between 2011 and 2017.

Following our assumption of the GPS signal interaction mainly being within the denser region of the eruption column, modelling columns as cylindrical obstacles whose core diameter is ~ 100 *m*, and assuming planar microwaves coming from the GPS satellites, we can consider Fraunhofer diffraction effects and the Babinet's principle [23] to constrain the maximum attenuation of GPS signal due to obstacles within ~ 10 *km* from the vent. This allowed discarding the distant GPS stations from the summit area in this analysis. Hence, we have analysed the SNR signals for all the 5 summit GPS stations on Mt. Etna to constrain the temporal normalization parameters in Eqs. (1)-(3) following the optimization step in (4) for both L1 and L2 bands. The resulting average of RMSE of optimally normalized SNR signals against the number of regressors is shown in Fig. 1. It is worth noting that the optimal number of regressors n (i.e. the smallest number of sidereal days considered in Equation (1) after which filtering does not enhance the signal significantly) is 2.

Estimating, for the last decades, in $1.13‰$ the mean fraction of time during which Mt. Etna is in paroxysmal activity, we set $\kappa = 3$ corresponding to the $1 - 1.13‰$ percentile of a standardized normal distribution (which is $\tilde{s}_{xy}(t)$ by definition in Eq. (1)). By applying the proposed methodology to the considered set of data, we have found that in six cases the anomalies in the SRN signal are well above the levels of casual fluctuations that can affect this kind of data and show narrow azimuthal dispersion. In these eruption cases, then, the Ψ_{x}^{f} set was not empty and thus we were able to identify the right position of the erupting vent, as shown in Fig. 2 where the vectors in Ψ_{x}^{f} and the active vent are plotted.

Figure 3 shows the time series of only the $\tilde{s}_{xy}(t)$ (in red) that intercept the erupting vent during the corresponding paroxysmal activity.

The characteristics of the eruptive episodes revealing evidences of anomalies in the SNR signals with the described method are rather diverse. The 23 October 2011 event was the seventeenth paroxysm in 2011 at the North-East Crater (NEC) and the volcanic plume was directed eastwards by low intensity winds (12 knots at 3000 m a.s.l.). The main explosive activity between 5 and 6 March 2013 occurred instead at the New South East Crater (NSEC), where the volcanic plume due to the lava fountain was dispersed by winds (35 knots at 3000 m a.s.l.) toward the NE. During the intense paroxysmal activity on the morning of 12 April, with the formation of discontinuous lava fountains, winds of about 30 knots at 3000 m a.s.l. dispersed volcanic plume in the atmosphere mainly towards the E-SE. The eruption column of the lava fountain on 23 November 2013 at the NEC reached 11 km a.s.l. and the plume was dispersed by strong winds (30 knots at 3000 m a.s.l.) toward the NE. On 3 December 2015, the paroxysmal event was produced from the Voragine crater (VOR) and formed eruption columns $>$ 11 km a.s.l.. The volcanic plume was dispersed by low intensity winds ($<$ 10 knots) toward the E and NE. Lastly, the activity of 18 May 2016, from the VOR crater, produced a volcanic plume that reach about 7 km a.s.l.. Volcanic ash was dispersed by SE winds of about 25 knots at 3000 a.s.l.

In order to study the sensitivity of the proposed method to its parameters, we evaluated the results using different values. In particular, by increasing the azimuthal dispersion level on the geometric filter (8) to $\pi/2$, the number of paroxysmal events for which the vent area was correctly identified doubles (see the supplementary material for further figures). The drawback of such easing of constraints is the loss of azimuth resolution in 3 cases out 13, which only allows identifying a wider area of the explosive activity and not the exact erupting vent, e.g. see Fig. 4. For the other parameter, κ, results indicate that a valid range for our case of study is between 2 and 4. Out of this range, the set Ψ_{x}^{f} may either include false anomalies or miss true ones. For the remaining fountains not detected by the proposed method, only $\sim 8\%$ were discarded because of geometrical filtering. For the others, the SNR signal did not show statistically significant variations (i.e. above the background noise) in strength.

V. Conclusion

We have presented a method to identify the erupting area during lava fountains by using GNSS data. Unlike previous

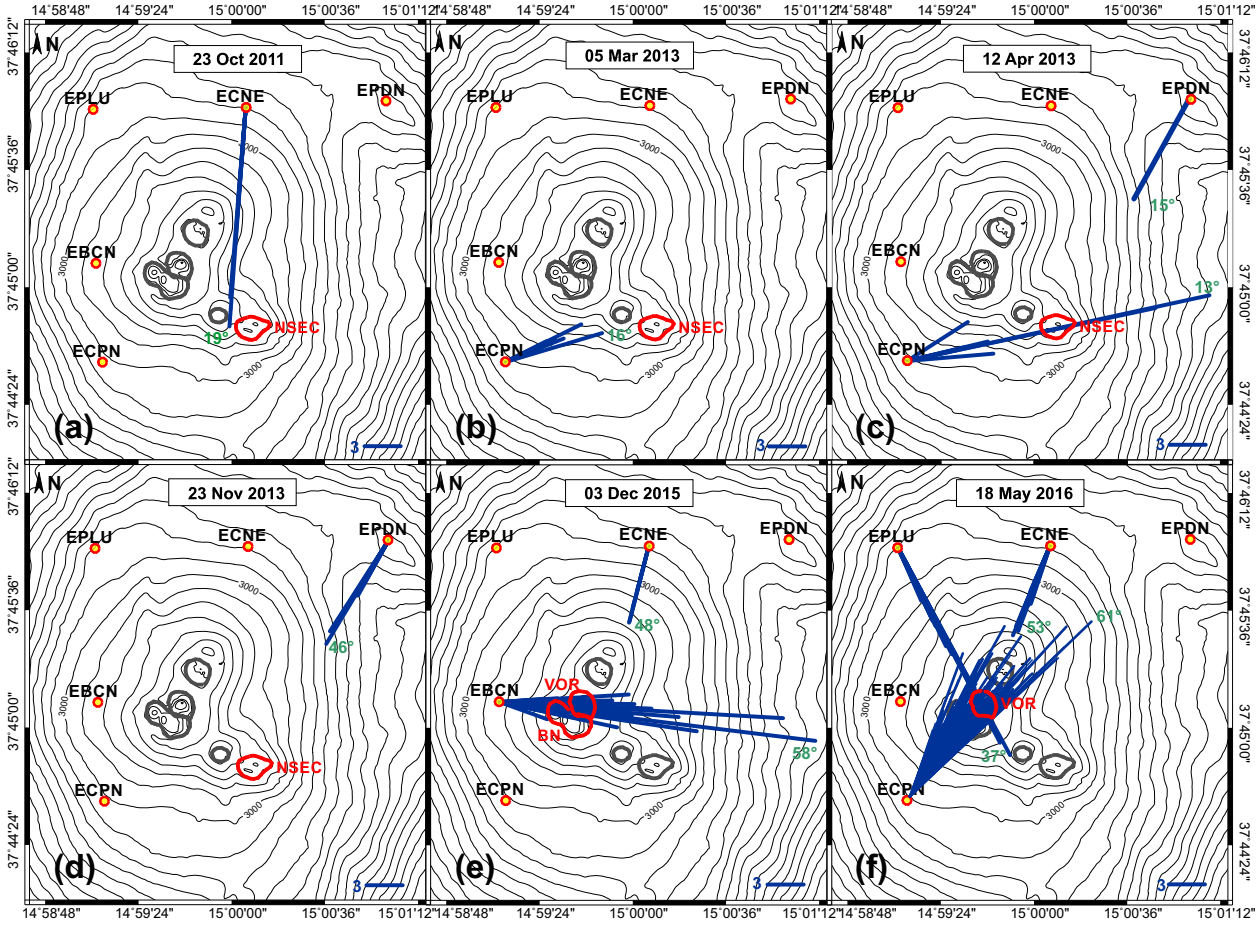

Fig. 2. In blue, the vectors Ψ_x^f during the lava fountain episodes for which the proposed filter highlights statistical anomalies in the GPS SNR signals. The thick red line indicates the corresponding erupting crater.

studies, we have analyzed a large dataset of volcanic paroxysms with different characteristics. Results suggest that, albeit not yet sufficiently robust, there is evidence of detectable interaction between volcanic plumes and GNSS signals. In particular, we have found that assuming the signature of this interaction is mainly linked to eruption columns, a geometrical analysis can, in favorable cases, allow detecting the erupting vent. The remaining negative cases suggest that further studies on the effects of the eruption column on SNR signals are needed to better characterize the physical parameters involved in the interaction/attenuation process. Nevertheless, the proposed method for erupting vent detection is flexible enough to be easily adapted to any other new methodology developed for anomaly detection in the GNSS signal. Since it is independent from the GNSS receiver, it can also be applied to any other volcano where a GNSS network is deployed. Thus, we are confident enough to promote this method as a complementary tool for volcano surveillance.

ACKNOWLEDGMENT

The authors would like to thank F. Donnadieu and M. Coltelli for the use of the Radar data that can be downloaded from the web-site http://wwwobs.univ-bpclermont.fr/SO/televolc/voldorad/voldo2b.php.

REFERENCES

[1] M. M. Scase, "Evolution of volcanic eruption columns," *Journal of Geophysical Research: Earth Surface*, vol. 114, no. F4, pp. n/a–n/a, 2009, f04003.

[2] R. S. J. Sparks, "The dimensions and dynamics of volcanic eruption columns," *Bulletin of Volcanology*, vol. 48, no. 1, pp. 3–15, 1986.

[3] R. Sparks, *Volcanic plumes*. Wiley, 1997. [Online]. Available: https://books.google.it/books?id=qt4SAQAAIAAJ

[4] M. Guffanti, J. W. Ewert, G. M. Gallina, G. J. Bluth, and G. L. Swanson, "Volcanic-ash hazard to aviation during the 20032004 eruptive activity of anatahan volcano, commonwealth of the northern mariana islands," *Journal of Volcanology and Geothermal Research*, vol. 146, no. 13, pp. 241 – 255, 2005, the 2003 Eruption of Anatahan Volcano, Commonweath of the Northern Mariana Islands.

[5] A. Neri, T. E. Ongaro, G. Macedonio, and D. Gidaspow, "Multiparticle simulation of collapsing volcanic columns and pyroclastic flow," *Journal of Geophysical Research: Solid Earth*, vol. 108, no. B4, apr 2003.

[6] T. Koyaguchi, Y. J. Suzuki, and T. Kozono, "Effects of the crater on eruption column dynamics," *Journal of Geophysical Research: Solid Earth*, vol. 115, no. B7, pp. n/a–n/a, 2010, b07205. [Online]. Available: http://dx.doi.org/10.1029/2009JB007146

[7] Y. J. Suzuki and T. Koyaguchi, "3-d numerical simulations of eruption column collapse: Effects of vent size on pressure-balanced jet/plumes," *Journal of Volcanology and Geothermal Research*, vol. 221222, pp. 1 – 13, 2012.

[8] D. Andronico, S. Scollo, and A. Cristaldi, "Unexpected hazards from tephra fallouts at Mt Etna: The 23 november 2013 lava fountain," *Journal of Volcanology and Geothermal Research*, vol. 304, pp. 118 – 125, 2015.

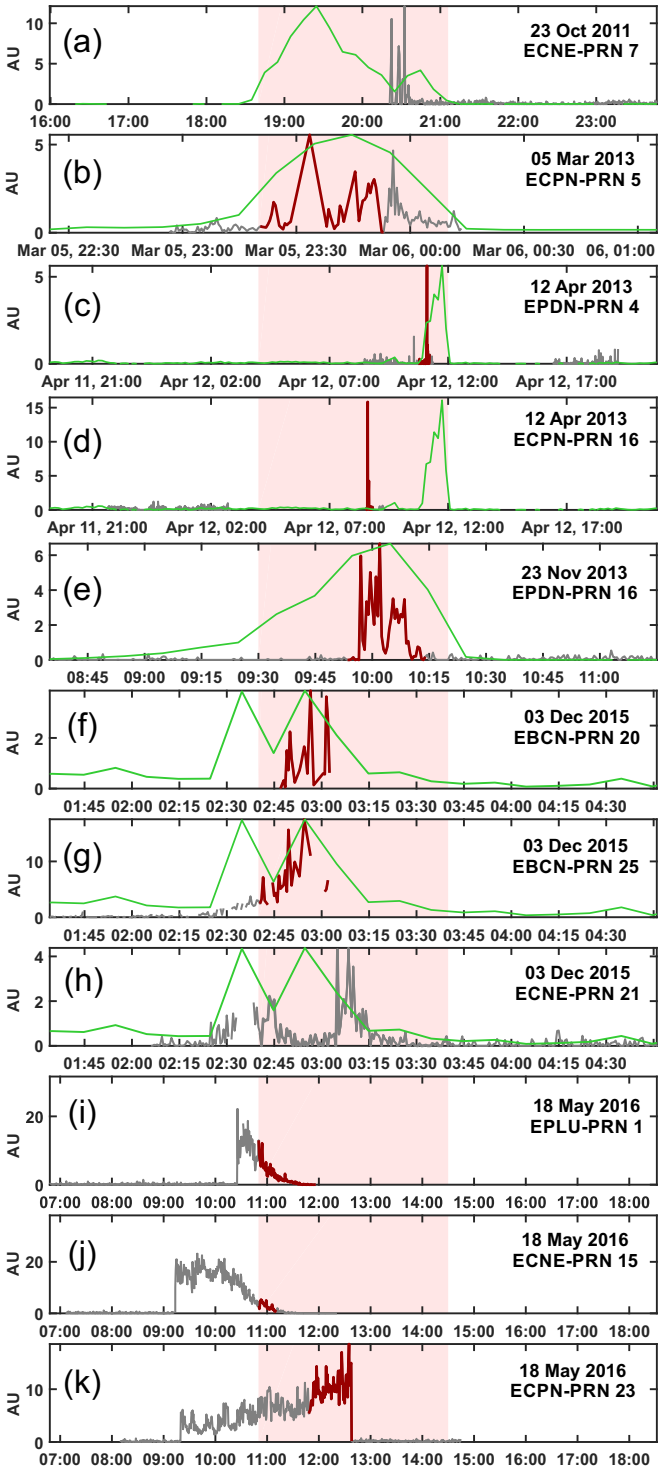

Fig. 3. In light red, the explosive episodes for which the proposed filter highlights statistical anomalies in the GPS SNR signals. In grey, the time series of $\tilde{s}_{xy}(t)$ during these fountain episodes, highlighted in dark red while intercepting the corresponding erupting vent. In green, the time series of radar backscattered power averaged every 10 minutes, normalized for the maximum $\tilde{s}_{xy}(t)$.

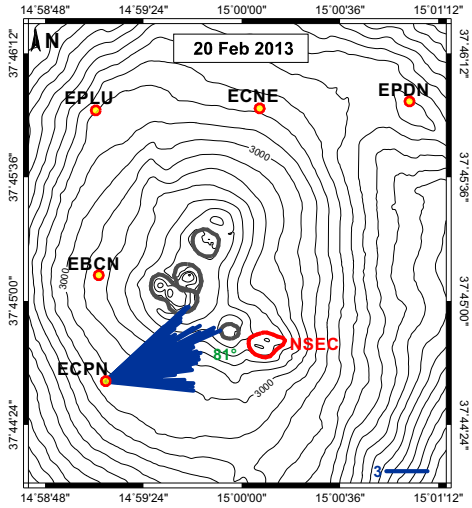

Fig. 4. In blue, the vectors $\Psi_{ECPN}^{20feb2013}$ with weaker azimuthal constraint during the lava fountain on 20 February 2013 for which the proposed filter highlights statistical anomalies in the GPS SNR signals. The thick red line indicates the corresponding erupting crater.

[9] G. D. Grazia, S. Falsaperla, and H. Langer, "Volcanic tremor location during the 2004 Mount Etna lava effusion," *Geophysical Research Letters*, vol. 33, no. 4, 2006.

[10] J. B. Johnson, "Source location variability and volcanic vent mapping with a small-aperture infrasound array at Stromboli volcano, Italy," *Bulletin of Volcanology*, vol. 67, no. 1, pp. 1–14, 2004.

[11] A. Cannata, P. Montalto, M. Aliotta, C. Cassisi, A. Pulvirenti, E. Privitera, and D. Patan, "Clustering and classification of infrasonic events at Mount Etna using pattern recognition techniques," *Geophysical Journal International*, vol. 185, no. 1, p. 253, 2011.

[12] J. Almendros, "Performance of the radial semblance method for the location of very long period volcanic signals," *Bulletin of the Seismological Society of America*, vol. 93, no. 5, pp. 1890–1903, oct 2003.

[13] M. Ripepe, E. Marchetti, and G. Ulivieri, "Infrasonic monitoring at Stromboli volcano during the 2003 effusive eruption: Insights on the explosive and degassing process of an open conduit system," *Journal of Geophysical Research: Solid Earth*, vol. 112, no. B9, pp. n/a–n/a, 2007, b09207.

[14] R. T. Modrak, S. J. Arrowsmith, and D. N. Anderson, "A Bayesian framework for infrasound location," *Geophysical Journal International*, vol. 181, no. 1, pp. 399–405, apr 2010.

[15] B. Andò and E. Pecora, "An advanced video-based system for monitoring active volcanoes," *Computers & Geosciences*, vol. 32, no. 1, pp. 85–91, feb 2006.

[16] K. M. Larson, "A new way to detect volcanic plumes," *Geophysical Research Letters*, vol. 40, no. 11, pp. 2657–2660, jun 2013.

[17] R. Grapenthin, J. T. Freymueller, and A. M. Kaufman, "Geodetic observations during the 2009 eruption of Redoubt Volcano, Alaska," *Journal of Volcanology and Geothermal Research*, vol. 259, pp. 115–132, jun 2013.

[18] M. Aranzulla, F. Cannavò, S. Scollo, G. Puglisi, and G. Immè, "Volcanic ash detection by GPS signal," *GPS Solutions*, vol. 17, no. 4, pp. 485–497, oct 2012.

[19] M. Aranzulla, F. Cannavò, and S. Scollo, "Detection of volcanic plumes by gps: the 23 november 2013 episode on Mt. Etna," *Annals of Geophysics*, vol. 57, no. Vol 57 (2014): Fast Track 2: Atmospheric emissions from volcanoes, Feb 2015.

[20] Y. Ohta and M. Iguchi, "Advective diffusion of volcanic plume captured by dense GNSS network around Sakurajima volcano: a case study of the vulcanian eruption on july 24, 2012," *Earth, Planets and Space*, vol. 67, no. 1, sep 2015.

[21] C. Textor, H. Graf, M. Herzog, J. Oberhuber, W. I. Rose, and G. Ernst, "Volcanic particle aggregation in explosive eruption columns. part i: Parameterization of the microphysics of hydrometeors and ash," *Journal of Volcanology and Geothermal Research*, vol. 150, no. 4, pp. 359 – 377, 2006. [Online]. Available: http://www.sciencedirect.com/science/article/pii/S0377027305002982

[22] S. Aoki, H. Kinoshita, B. Guinot, G. Kaplan, D. D. McCarthy, and P. K. Seidelmann, "The new definition of universal time," *Astronomy and Astrophysics*, vol. 105, pp. 359–361, 1982.

[23] M. Born and E. Wolf, *Principles of Optics: Electromagnetic Theory of Propagation, Interference and Diffraction of Light (7th Edition)*, 7th ed. Cambridge University Press, 1999.